Experiments and simulations on hot expanded boron

Jean Clérouin,* Patrick Renaudin, and Pierre Noiret
Département de Physique Théorique et Appliquée, CEA/DAM Île-de-France, Bruyères-le-Châtel 91297 Arpajon Cedex, France
(Received 21 December 2007; published 28 February 2008)

We measured the thermodynamical and transport properties of boron in the warm dense matter regime ($15\,000\ \mathrm{K} < T < 25\,000\ \mathrm{K}$ and $\rho = 0.094\ \mathrm{g/cm^3}$). Experimental data are compared with quantum molecular dynamics (QMD) simulations. We find a very good agreement between data and calculations, which permits us to transform experimental energies into temperatures, and allows us to compare conductivities with an average atom model coupled with a Kubo-Greenwood calculations. Contact is made between computationally intensive QMD simulation codes and fast average atom models.

DOI: 10.1103/PhysRevE.77.026409 PACS number(s): 52.25.−b, 52.65.−y, 52.50.−b, 52.70.−m

I. INTRODUCTION

The transition between the condensed state of matter and the plasma state has not been studied much because of the difficulty to precisely model the properties of matter in this regime. When a sample is heated by a pulsed electrical discharge, it encounters first a melting transition followed by a liquid to gas transition. The heated vapor gets ionized and eventually forms a plasma. If the plasma is confined, as it is in this experiment, the final thermodynamic state is characterized by a coupling parameter and a degeneracy parameter of order of unity, making any small parameter expansion useless. This region, which is also referred to as warm dense matter is very challenging for models, and corresponds to the so-called interpolation region for the SESAME database [1].

Since the pioneering work of DeSilva [2], measuring discharges confined by water, there have been very few experiments dealing with pulsed electrical discharges. Recently Korobenko *et al.* [3,4] used dynamically confined discharges to produce plasmas. In all of these experiments, however, an external model is needed [equation of state or magnetohydrodynamics (MHD) code] to extract the data, in contrast with this experiment. In the "Enceinte à Plasma Isochore" (EPI), the electrical pulsed discharge is confined, at constant volume. Voltages, intensities, and, hence, resistivities, as well as pressures are directly obtained. With a simple assumption relative to the radiative losses in the confinement device, energies are deduced. Experiments were performed on metals, such as aluminum [5,6], copper [7], gold [8], or titanium. In such experiments a metal-nonmetal (MNM) transition was observed at the beginning of the discharge, which is common when a metal expands [9], followed by a rise of the conductivity with the temperature in the plasma phase. It has been argued that this MNM transition was linked to the vicinity of the critical point of the metals, which are not known precisely. We have shown that quantum molecular dynamics (QMD) simulations were particularly suited to describe this difficult regime due to their ability to simultaneously predict the equation of state and the transport properties, without any assumption on the species involved or in the ionization state.

In this paper, we present results on boron plasma obtained by the same scheme. The difficulty here is that we start from a quasi-insulator in the solid phase. Crystalline boron has a very complex structure and even the liquid phase remains complex [10]. The initiation of the discharge is difficult and requires the help of an aluminum wire to start the process. In contrast with good metals, however, the liquid phase of boron is much more conducting than the solid phase. Usually when a metal melts, its conductivity is divided by a factor of 1.5 to 2. Here the conductivity at melting is comparable with a metal, a behavior already observed for semiconductors such as silicium [11]. The electrical conductivity of liquid boron itself is poorly known due to the difficulty of the experiments. The most recent experiment of Glorieux [12] gives a conductivity of $0.96 \times 10^3\ [\Omega\ \mathrm{cm}]^{-1}$ and a first QMD simulation of Vast *et al.* [13], $25 \times 10^3\ [\Omega\ \mathrm{cm}]^{-1}$ [14].

The paper is organized as follows. In the next section we describe the experimental setup with a particular emphasis on the initiation of the electrical discharge with a boron sample. We then describe the simulations and we give some details on the computation of the electrical conductivity. Experimental data are compared with simulation results in Sec. IV and a relation between energies and temperatures is deduced. In Sec. V, we compare with an average atom (AA) model and conclude with an estimation of the ionization.

II. EXPERIMENTS

The experiments were conducted with the EPI facility, which has been described in detail in previous papers [5,6]. This facility allows absolute measurements of the pressure and conductivity without the help of any external models. The amount of matter in the chamber yields the exact density of the plasma which, due to the slowness of the discharge ($250\ \mu\mathrm{s}$) is nearly homogeneous, as checked by x-ray measurements. The plasma heating is assumed to be done along an isochore. Two piezoelectric sensors with $2\ \mu\mathrm{s}$ rise time are placed at each end of the sapphire tube to measure the pressure during the discharge. The sensors are acceleration compensated and allow one to measure a maximum pressure (0.7 GPa) lower than the plasma pressure. There is no contact between them and the plasma. A surface divider piston reduces by a factor of 4 the applied pressure and transmits it to the sensor. A dynamic and static calibration was performed before each experiment. The electrical conductivity is deduced from the time evolution of current and voltage.

*jean.clerouin@cea.fr

TABLE I. Main constituents and impurities. X_M and x_N are the proportions in masses and in numbers of atoms and ρ_i are the partial densities.

Element	Mass g	N 10^{19}	x_M %	x_N %	ρ_i g/cm^3
B	1.9785	11 028	98.24	99.46	0.0916
Al	0.0253	56	1.28	0.51	0.0012
W	0.0102	3.3	0.52	0.03	0.0005

Note that all quantities are known versus the internal energy variation; to preserve the absolute character of our data we will show them this way (see Figs. 2 and 3). The internal energy variation δU can be evaluated from the electrical energy input E_{el} and is given by $\delta U=(E_{\mathrm{el}}-E_{\mathrm{rad}})+\delta W$, where E_{rad} is the thermal losses at the vessel walls. The mechanical work loss δW due to the vessel expansion under pressure is less than 1% of E_{el} and can be neglected. The thermal losses are assumed to be radiative during the plasma phase, and negligible before. Radiative losses of a blackbody of surface S are given by $dE_{\mathrm{rad}}/dt=\sigma\times S\times(T^4-T_0^4)$, where σ is the Stefan-Boltzmann constant and T_0 is the ambient temperature. The uncertainties in the measurements of the conductivity are related to the accuracy of current and voltage measurements and are estimated to be about 15%. The uncertainty in the internal energy variation is a little bit more complex to estimate, due to the ablation of the internal channel containing the plasma, but can be also estimated at about 15%.

Boron is a special case because, in contrast with previous studies with metals, the material in the chamber can be considered as a semiconductor, with a conductivity of a few 10^{-7} $(\Omega\ \mathrm{cm})^{-1}$. Such a resistivity does not permit a proper start of the electrical discharge. To initiate the discharge, we have tighten a bundle of 151 boron fibers of 200 μm in diameter and 19.1 cm in length, with an aluminum wire of 250 μm diameter. The mass of the aluminum wire is 25 mg. Moreover, each boron fiber contains a tungsten core of 5 μm diameter [15], giving a total mass of tungsten for the bundle of 10 mg. We have thus 10 mg of tungsten, 25 mg of aluminum, and 1.978 g of boron, which corresponds to a proportion in mass of 0.5% for tungsten and 1.3% for aluminum, and in number of atoms of, respectively 0.03% for tungsten and 0.51% for aluminum (see Table I). Such a low concentration (3 atoms of tungsten and over 11 028 atoms of boron) is far beyond the actual possibilities of *ab initio* simulations, and hence we will neglect the effects of the tungsten core and of the aluminum wire for QMD simulations. In the following, we will assume that the total density of the system is 0.094 g/cm^3 of pure boron.

The record of pressures and total resistance versus time is shown in Fig. 1. In the first microseconds we observed a burst of the resistance, with a slight bump in the pressure. This corresponds to the explosion of the aluminum wire which induces the discharge into the boron up to the melting indicated by the arrow labeled M. As the boron sample turned to liquid, the resistance goes to a minimum of about 0.05 Ω that corresponds to a conductivity of 7×10^3 $[\Omega\ \mathrm{cm}]^{-1}$, if we suppose a constant volume melting of the bundle of boron fibers. This number stays in qualitative agreement with estimations of liquid boron conductivity previously given but is probably overestimated due to the pollution of the aluminum plasma. At a time of about 150 μs, indicated by the arrow labeled B, the vaporization starts and the insulating atomic vapor fills up the whole volume. At this time we observed a luminescent discharge and the resistance again diminished with the temperature and increasing ionization. At 320 μs we observed a sudden drop in the resistance attributed to a short circuit in the confinement structure. After a maximum in the pressure, the system cooled down. To ensure a good quality of the measurements, data were taken between 230 and 310 μs, in the plasma phase as indicated by the two vertical lines.

III. SIMULATIONS

In the thermodynamical regime of interest ($\rho\simeq\rho_0/10$ and 5000 K$<T<$40 000 K), Quantum molecular dynamics (QMD) simulations have shown their efficiency for predicting simultaneously both thermodynamics properties and transport properties [8]. Despite some well-known limitations at high temperatures (beyond 5 eV) resulting from the use of pseudopotentials and the number of states that can be included, the QMD method is particularly suited to describe various situations in the WDM regime.

The simulations were performed using PAW pseudopotentials [16] with the electronic structure package VASP devel-

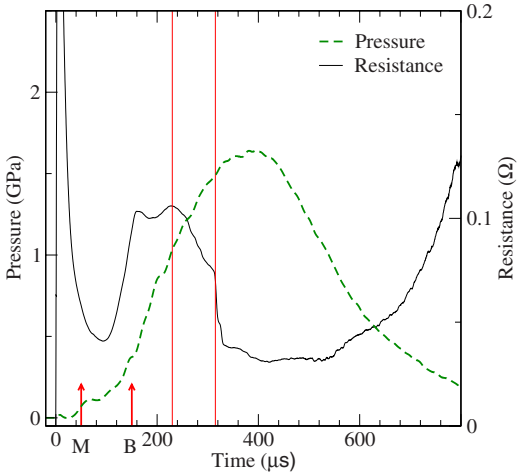

FIG. 1. (Color online) Pressure and resistance versus time. Time of melting (m) and boiling (b) of the boron sample are indicated by arrows. Data are taken between the two vertical lines.

TABLE II. QMD simulations of boron at a density of 0.094 g/cm^3.

Energy MJ/kg	Pressure GPa	Temperature K	σ_{dc} 2^3 $(\Omega\ cm)^{-1}$	σ_{dc} 3^3 $(\Omega\ cm)^{-1}$
78.6	0.804	15 000	84	75.4
90.2	1.16	17 500	130	136
96.5	1.26	18 750	167	167
98.0	1.414	20 000	190	192
102.7	1.537	21 250	217	218
109.2	1.726	22 500	246	237
121.0	2.056	25 000	283	276
127.0	2.221	26 250	318	319

oped at the University of Vienna [17]. We used a PAW pseudopotential with three active electrons ($2s^2 2p^1$) with a cutoff energy of 318 eV. Inclusion of more electrons is only needed at very high pressure as shown in a previous paper [18], when core electrons are subject to ionization.

The exchange and correlation terms were treated at the level of the LDA approximation [19] and using the Ceperley-Alder parametrization [20]. During the molecular dynamics simulations, the Brillouin zone was sampled at the Γ point, whereas we used more refined k-point sampling such as 2^3 and 3^3 in the Monkhorst-Pack scheme [21], for the optical calculations. The ionic trajectories were generated for 16 atoms of boron during 1000 time steps of 0.2 fs after equilibration. Molecular dynamics simulations were performed in the isokinetic ensemble (constant temperature) in order to ensure an easier control of the temperatures. For each temperature, the initial conditions were taken from a previous simulation performed at lower temperature to speed up the equilibration time. We assume that we reach equilibrium when records of pressures versus time are showing a steady average and enough oscillations around the average value (5 to 10 oscillations). We also tested the convergency of the simulations with the number of atoms by running 32 ions simulations, without noticeable changes. Uncertainties in the pressure (errors bars) are obtained by statistical fluctuations along the MD run.

From the knowledge of the Kohn-Sham orbitals ψ_n, energies ϵ_n, and occupations f_n, the conductivity was computed using the Kubo-Greenwood formulation [22,23] on selected ionic configurations

$$\sigma(\omega) = \frac{2\pi}{3\omega}\frac{1}{\Omega}\sum_{n,m,\alpha}\sum_{\mathbf{k}} W(\mathbf{k})(f_n - f_m) \times |\langle \psi_n^{\mathbf{k}}|\nabla_\alpha|\psi_m^{\mathbf{k}}\rangle|^2 \delta(\epsilon_m^{\mathbf{k}} - \epsilon_n^{\mathbf{k}} - \hbar\omega), \quad (1)$$

where $\mathbf{k}$ and $W(\mathbf{k})$ are the vectors and the weight in the Brillouin zone, ∇_α is the velocity operator in each direction ($\alpha = x, y, z$) between two states n and m with occupation f_n and f_m. The dc conductivity is obtained by taking the zero frequency limit of $\sigma(\omega)$.

To compute the reference state of energies, we simulated the solid at 300 K, in the β phase of boron with 105 atoms in the primitive cell. We got an energy per atom of −7.322701 eV/atom, which must be subtracted from the energies given by QMD simulations. Results of QMD simulations are given in Table II.

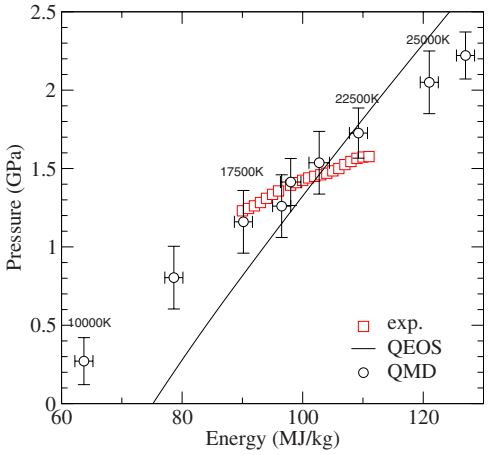

FIG. 2. (Color online) Pressure versus internal energy. Experimental data (red squares) and QMD simulations (circles). Temperatures of selected QMD simulations corresponding to Table II are indicated.

IV. RESULTS

The equation of state (pressure versus internal energy) is shown in Fig. 2. We get a reasonable agreement between the QMD simulations and the experimental data. In the experimental region (between 90 and 110 MJ/kg) the agreement with the model quotidian equation of state [24] (QEOS) is rather good, but we get a systematic underestimation at lower energy and overestimation at higher energy.

The same observation holds for the electrical conductivity shown in Fig. 3. The comparison of conductivities computed with 2^3 and 3^3 **k** point sampling shows a very weak dependency. This conductivity is one order of magnitude lower than the liquid conductivity, but with a temperature dependency characteristic of a semiconductor.

Although we observe a reasonable overall agreement for pressures and conductivities, between QMD and experimen-

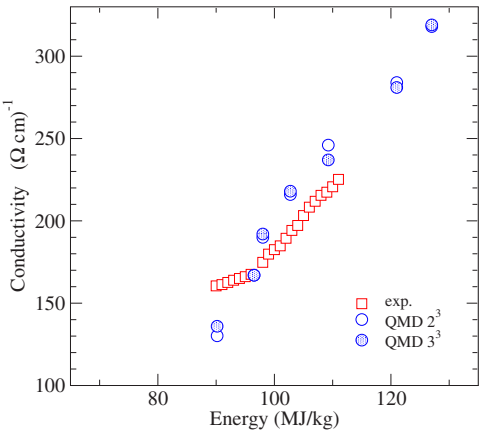

FIG. 3. (Color online) Electrical conductivity versus energy.

TABLE III. Experimental results. Temperature are computed with the help of relation (2).

Energy MJ/kg	Pressure GPa	Resistivity 10^{-3} (Ω cm)	Conductivity $(\Omega\ \mathrm{cm})^{-1}$	Temperature K
90	1.23	6.23	160.5	17 753
91	1.245	6.20	161.3	18 000
92	1.262	6.15	162.6	18 253
93	1.283	6.1	163.9	18 500
94	1.310	6.06	165.0	18 754
95	1.335	6.02	166.1	19 000
96	1.357	5.97	167.5	19 254
97	1.377	5.85	170.9	19 500
98	1.394	5.72	174.8	19 754
99	1.410	5.56	179.8	20 000
100	1.425	5.48	182.5	20 255
101	1.440	5.41	184.8	20 500
102	1.425	5.28	189.4	20 755
103	1.460	5.15	194.2	21 000
104	1.470	5.07	197.2	21 255
105	1.485	4.92	203.2	21 500
106	1.5	4.80	208.3	21 755
107	1.525	4.72	211.9	22 000
108	1.545	4.64	215.5	22 256
109	1.565	4.60	217.4	22 500
110	1.573	4.53	220.7	22 756
111	1.576	4.44	225.2	23 000

tal data, we note a change in the experimental data slope at an energy of 96 MJ/kg. A careful examination of the raw electrical data shows very small short-circuit signals at a time corresponding to this energy. These events are interpreted as leaks of plasma through the composite structure. This effect is very weak, but explains that the experimental pressures and conductivities are probably underestimated by less than 5% for the highest energy.

Knowing the temperatures of QMD simulations, and because of the good agreement between simulations and experimental data, we built a fit to translate energies into temperature. This fit reads

$$T(\mathrm{K}) = -4758 + 250.13E \ \ (\mathrm{MJ/kg}). \tag{2}$$

Temperatures corresponding to the experimental data are given in Table III. In Fig. 4, the pressure is now plotted versus temperature. In this representation we see that QEOS yields too high pressures due to an overestimation of the ionization. It must be noted that the perfect gas yields a good description of the pressures in the experimental range, in contrast with gold [8], where the perfect gas very quickly underestimated the experimental data. Outside the experimental range, QMD calculations can help to interpret the equation of state. Below 17 000 K, the QMD pressures are lower than the perfect gas. We explain this effect by a tendency to a dimerization prefiguring the gas-liquid transition

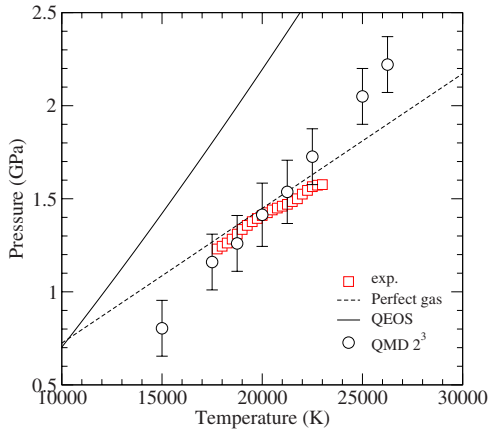

FIG. 4. (Color online) Pressure versus temperature using fit (2).

at lower temperature. Let us recall that the critical point of boron is estimated to be $\rho=0.69$ g cm^{-3}, $P=0.956$ GPa, and $T=8000$ K [25]. Over 25 000 K, the QMD pressures are higher than the perfect gas, which can be understood as the onset of ionization, with an average ionization fraction lying between 0.1 and 0.3.

The optical conductivities shown in Fig. 5 exhibit the usual trends already observed for hot expanded metals. First, the zero-frequency value of $\sigma(\omega)$ which yields the dc electrical conductivity, increases with temperature and a Drude behavior emerges at low energy. Second, we observe a well defined peak at low temperature which will be identified unambiguously later as the $2s$-$2p$ transition. In contrast with metals, the position of this peak is almost constant due to low ionization. For copper, due to the competition of neutral and singly ionized species, the peak was moving toward high densities with temperature. A Drude fit of the optical conductivity in the low-energy range ($\hbar\omega<2$ eV) is obtained by adjusting the relaxation time to get the best fit of the optical conductivities, for a given dc conductivity σ_{dc}

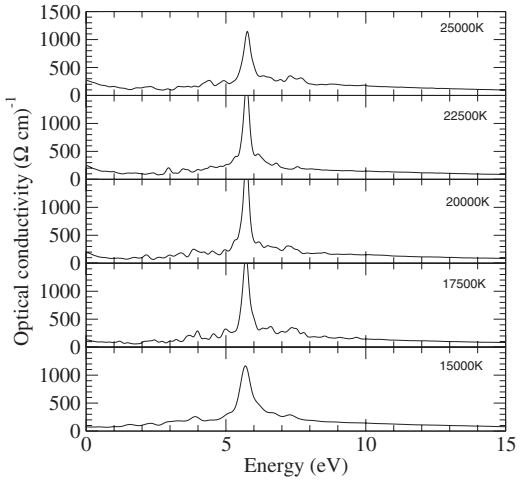

FIG. 5. Computed optical conductivities versus energies for selected temperatures.

TABLE IV. Electrical conductivities given by the Johnson model compared with a Ziman formulation. Ionization are computed with the AA model (Z_{AA}) and a Drude fit of the low-frequency part of the electrical conductivity (Z_D) with a collision time τ.

Temperature K	KG $(\Omega\ \mathrm{cm})^{-1}$	Ziman $(\Omega\ \mathrm{cm})^{-1}$	Z_{AA}	Z_D	τ $\times 10^{-15}$ s
17 500	97	353	0.12	0.07	1.3
18 750	119	400	0.14	0.08	1.3
20 000	153	446	0.17	0.10	1.3
21 250	165	486	0.19	0.12	1.2
22 500	196	538	0.23	0.12	1.2
25 000	255	629	0.29	0.14	1.3
26 250	285	671	0.32	0.14	1.5

$$\sigma(\omega) = \frac{\sigma_{\mathrm{dc}}}{1+\omega^2\tau^2}. \tag{3}$$

From this fit we can compute the density of carriers using $n_e = m_e\sigma_{\mathrm{dc}}/\tau e^2$ and extract an ionization Z_D and a collision time τ coherent with the electrical conductivity. Z_D and τ are given in Table IV. We emphasize that in the case of boron, the Drude peak at zero frequency is very weak, which leads to important errors in the calculation of Z_D. We estimate the error to be around 20%.

V. AVERAGE ATOM APPROACH

QMD simulations in this hot expanded regime are rather expensive. It is thus desirable to have a more efficient tool to predict the plasma properties much faster. Such a goal was recently achieved by Johnson *et al.* [26], who proposed to couple an average atom description of the atomic physics with a Kubo-Greenwood calculation of the conductivity (KGAA), instead of using the usual Ziman approach. In this model, the number of free electrons and the atomic levels are obtained through an atomic model and a Kubo-Greenwood calculation gives bound-bound, bound-free contributions that are added to a Drude description for free electrons. The relaxation time is adjusted until the conductivity sum rule is obtained. The different contributions to the optical spectrum are shown in Fig. 6(a). The two bound-bound contributions, predicted by the KGAA model, are $2s$-$2p$ at 5.64 eV and $1s$-$2p$ at 174 eV. Close to those values but characterized by an edge are the photoionization contributions.

All contributions are summed up and compared with the QMD spectrum in Fig. 6(b). The location and the overall profile of the $2s$-$2p$ transition agrees with the QMD calculation. The predicted $1s$-$2p$ is out of the range of energy described by the three-electron pseudopotential. The KGAA dc conductivities shown in Fig. 7 and given in Table IV are in good agreement with experiments and appear a little lower than the QMD calculation (by less than 5%). In this regime, a Ziman calculation of the electrical conductivity overestimates the experimental dc conductivity by a factor of 3, as shown in Fig. 7. This overestimation can be traced back to the estimation of the number of free electrons (the ionization) entering the Ziman formula. In Table IV we show the ionization predicted by the AA model, the ionization deduced from the Drude fit of the optical conductivities (Z_D) given by Eq. (3). The fact that Z_{AA} is always greater than the Drude estimation explains the overestimation of the Ziman formulation of the electrical conductivity. In this experiment the ionization is thus rather small (of order of 0.1–0.3) which explains that the electrical conductivities are smaller by a factor of 2 compared to the conductivities measured for gold in the same energy range [8]. The coupling parameter $\Gamma = Z^2e^2/ak_BT$, where a is the ionic mean sphere radius, is thus between 0.13 for $Z=0.2$ and 0.3 for $Z=0.3$ and the degeneracy parameter $\theta = T/T_F$ is 0.3 at this density. The system is then moderately coupled and partially degenerate which corresponds to the WDM regime.

To estimate the effect of aluminum and tungsten impurities on the electrical conductivities we have carried out KGAA calculations on aluminum and tungsten at partial densities of, respectively, 0.0012 $\mathrm{g/cm^3}$ and 0.0005 $\mathrm{g/cm^3}$. For aluminum we found a dc conductivity of the same order than

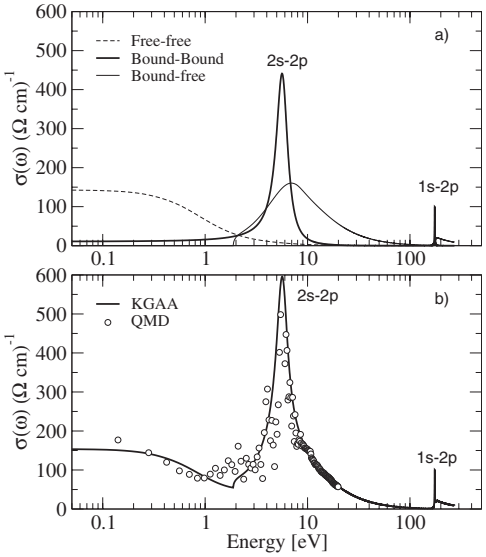

FIG. 6. Optical spectra at 20 000 K. (a) KGAA model with free-free (dashed line), bound-bound (heavy line), and bound-free contributions (full line). (b) Comparison of the full spectrum (heavy line) with QMD simulation (circles).

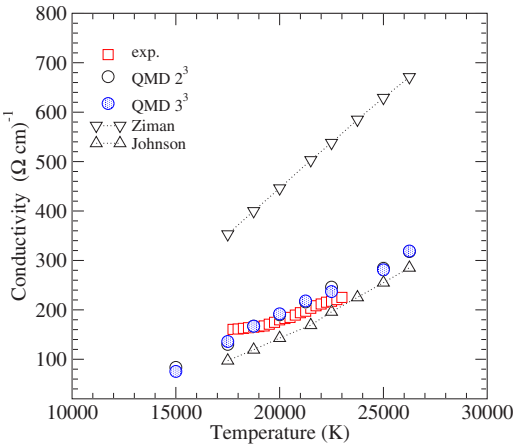

FIG. 7. (Color online) Electrical conductivity versus temperature.

boron [143 $(\Omega\,\mathrm{cm})^{-1}$ at 20 000 K, see Table IV] which combined with the boron conductivity yields no contributions. We showed that in near perfect gas regimes, a good estimation of the conductivity of the mixture can be obtained by a simple atomic fraction combination of conductivities [27]. For tungsten, we found a very low conductivity, due to the quasi-isolated atom state, which combined with a vanishing atomic fraction also yields no contribution. We conclude to the absence of pollution effects in the homogeneous plasma phase, when data are recorded. The effect of aluminum is more important in transient heating phases, which was precisely the idea of using aluminum to start the discharge.

VI. CONCLUSION

We have performed experiments on hot expanded boron in a range of temperatures 15 000 K$<T<$25 000 K at a constant density of 0.094 $\mathrm{g/cm^3}$. We measured the pressure and the electrical conductivity in an absolute way and deduced the variation of energy with a simple assumption on thermal losses. We found a very good agreement with quantum molecular dynamics simulations for pressures and resistivities versus energies. From the knowledge of the temperatures of QMD simulations, and from a fit, we have been able to deduce experimental temperatures. We have also obtained the electrical conductivity with the help of a Kubo-Greenwood version of an average atom model. This approach leads to much better results than the usual Ziman approach usually made for plasmas.

ACKNOWLEDGMENTS

We are very grateful to W. Johnson for providing his average atom code, as well as B. Siberchicot for giving a boron β configuration and for fruitful conversations. A. Rakhel is thanked for constructive discussions. We also thank B. Loffredo for the mechanical work on the experiment.

[1] S. P. Lyon and J. D. Johnson, SESAME, The Los Alamos National Laboratory Equation of State Database, Report No. LA-UR-92-3407 (1992).
[2] A. W. De Silva and J. D. Katsouros, Phys. Rev. E **57**, 5945 (1998).
[3] V. N. Korobenko, A. D. Rakhel, A. I. Savvatimski, and V. E. Fortov, Phys. Rev. B **71**, 014208 (2005).
[4] V. N. Korobenko and A. D. Rakhel, Phys. Rev. B **75**, 064208 (2007) in this last paper, the expansion of the plasma is calculated through a fully one-dimensional analytical model. An assumption is still made on the equation of state of sapphire.
[5] V. Recoules, P. Renaudin, J. Clérouin, P. Noiret, and G. Zérah, Phys. Rev. E **66**, 056412 (2002).
[6] P. Renaudin, C. Blancard, J. Clérouin, G. Faussurier, P. Noiret, and V. Recoules, Phys. Rev. Lett. **91**, 075002 (2003).
[7] J. Clérouin, P. Renaudin, Y. Laudernet, P. Noiret, and M. P. Desjarlais, Phys. Rev. B **71**, 064203 (2005).
[8] P. Renaudin, V. Recoules, P. Noiret, and J. Clérouin, Phys. Rev. E **73**, 056403 (2006).
[9] F. Hensel and W. W. Warren, Phys. Scr. **25**, 283 (1988).
[10] S. Krishnan, S. Ansell, J. J. Felten, K. J. Volin, and D. L. Price, Phys. Rev. Lett. **81**, 586 (1998).
[11] I. Štich, R. Car, and M. Parrinello, Phys. Rev. B **44**, 4262 (1991).
[12] B. Glorieux, M. L. Saboungi, and J. E. Enderby, Europhys. Lett. **56**, 81 (2001).
[13] N. Vast, S. Bernard, and G. Zérah, Phys. Rev. B **52**, 4123 (1995).
[14] The value given by Vast *et al.* is probably strongly overestimated due to an approximated definition of the velocity operator in the Kubo-Greenwood formulation.
[15] Monofilaments of boron are provided by GoodFellow under reference B005915. They are made of a 5 microns tungsten core on which boron is condensed to form a filament of 200 microns in diameter.
[16] G. Kresse and D. Joubert, Phys. Rev. B **59**, 1758 (1999).
[17] G. Kresse and J. Hafner, Phys. Rev. B **47**, 558 (1993).
[18] S. Mazevet, F. Lambert, F. Bottin, G. Zérah, and J. Clérouin, Phys. Rev. E **75**, 056404 (2007).
[19] The choice between LDA and GGA was decided by computing equilibrium properties of solid boron in β phase. Moreover, we believe that at high temperature the effect of the exchange correlation approximation becomes less crucial.
[20] D. M. Ceperley and B. J. Alder, Phys. Rev. Lett. **45**, 566 (1980).
[21] H. J. Monkhorst and J. D. Pack, Phys. Rev. B **13**, 5188 (1976).
[22] R. Kubo, J. Phys. Soc. Jpn. **12**, 570 (1957).
[23] D. A. Greenwood, Proc. Phys. Soc. Jpn. **71**, 585 (1958).
[24] R. M. More, K. H. Warren, D. A. Young, and G. B. Zimmerman, Phys. Fluids **31**, 3059 (1988).
[25] V. E. Fortov, I. T. Iakubov, and A. G. Khrapak, *Physics of Strongly Coupled Plasma* (Oxford University Press, Oxford, 2006), Vol. 135.
[26] W. R. Johnson, C. Guet, and G. F. Bertsch, J. Quant. Spectrosc. Radiat. Transf. **99**, 327 (2006).
[27] J. Clérouin, V. Recoules, S. Mazevet, P. Noiret, and P. Renaudin, Phys. Rev. B **76**, 064204 (2007).